On the dynamics of axisymmetric turbulent separating/reattaching flows

Pierre-Élie Weiss,[1] Sébastien Deck,[1,a)] Jean-Christophe Robinet,[2] and Pierre Sagaut[3]
[1]*Department of Applied Aerodynamics, ONERA, Meudon FR-92190, France*
[2]*SINUMEF, Arts et Métiers, ParisTech, 75013 Paris, France*
[3]*Institut Jean Le Rond d'Alembert, Université Pierre et Marie Curie, 75252 Paris Cedex 05, France*

(Received 27 October 2008; accepted 30 May 2009; published online 20 July 2009)

The present work focuses on the intrinsic properties of an axisymmetric separating/reattaching flow. A numerical simulation of a compressible flow over a cylinder extended by another cylinder of smaller diameter is performed at a Reynolds number based on free stream velocity U_∞ and on the diameter of the larger cylinder D of 1.2×10^6. Statistical and fluctuating properties are scrutinized and compared with the available experimental data. Especially, experimental wall pressure coefficient and rms pressure fluctuations are well-reproduced by the simulation. A large scale coherent motion associated to $fD/U_\infty\approx0.2$ rules the organization of the flow. Moreover, these properties are linked to a linear stability analysis coupled with a two-point correlation analysis unveiling the major importance of highly coherent antisymmetric modes in the flow behavior. Finally, the axisymmetric body dynamics seems to be led by a significant absolutely unstable area suggesting a global instability mechanism. © *2009 American Institute of Physics*.
[DOI: 10.1063/1.3177352]

I. INTRODUCTION

Unsteady flow mechanisms such as wall-bounded turbulent shear phenomena with separation and reattachment have been studied for decades. Among them, axisymmetric and plane step flows can be distinguished. As emphasized by Deck and Thorigny,[1] axisymmetric step flows present similarities with plane facing step flows regarding the shear layer instability process. Plane flows featuring separation from a leading edge have been extensively studied in the past both numerically and experimentally. Nevertheless, it is observed in literature that less attention was paid to the analysis of axisymmetric configurations than to their plane counterpart. Actually, the amount of unsteady analysis and experimental data about axisymmetric afterbody flows is very limited in literature. A few authors investigated the disparities between plane and axisymmetric afterbodies. Roshko[2] stressed the lack of a theory analogous to the one of Von Kàrmàn for the plane vortex street, Calvert[3] studied the flow past cones and observed discrepancies regarding the periodic shedding prominence, and Gai and Patil[4] assessed the loss of efficiency of a subsonic blunted axisymmetric base controlled by several devices known to yield significant drag reduction in similar two-dimensional flows. On the experimental side, Délery and Siriex[5] reviewed results about intricate axisymmetric afterbodies and showed that the wall pressure distribution was dramatically influenced by the geometry. More recently, Deprés *et al.*[6] highlighted the features of several axisymmetric base flows, depending on the occurrence of a downstream solid reattachment of the free shear layer or not.

Such flows are known to feature highly coherent structures (Ref. 7) linked to the Von Kàrmàn shedding process. The organized motions in turbulent flows have a long history, dating from 1940s, and extensive presentations of earlier works can be found in surveys of Laufer,[8] Cantwell,[9] and Ho and Huerre.[10] It has been recognized that the harmonic perturbations in turbulent shear flows are governed by an instability mechanism, which has triggered a number of theoretical models within the scope of the linear stability theory of turbulent flows (Refs. 11–15). Moreover, Sandberg and Fasel[16] investigated numerically the instability mechanisms in supersonic axisymmetric wakes behind a bluff body for several Reynolds numbers and they finally related unstable modes to coherent structures. Finally, Deck and Thorigny[1] conjectured the existence of an absolute unstable area in the middle of the recirculation zone on the present axisymmetric configuration but in the case of a supersonic jet.

Considering all that has been said before, it seems of interest to couple the unsteady analysis with the linear stability theory after a preliminary validation of the simulation with the available experiments. To achieve this purpose, this article is organized as follows: characteristics of the tested configuration and numerical aspects of the simulation are given in Sec. II. The governing equations and the associated numerical method used to perform the linear stability analysis are also mentioned. Section III displays results in terms of instantaneous and mean fields validating the simulation at the same time with the available experimental data. Then, a spectral analysis exhibits frequencies of interest with their spatial distribution supporting, at last, a local linear stability analysis determining the convective or absolute nature of the instability in the mixing layer zone.

II. METHODS AND CONFIGURATION SETUP

The axisymmetric afterbody dimensions (see Fig. 1) were chosen to dovetail with the experiments of ONERA's S3Ch continuous research wind tunnel described by Deprés *et al.*[6] and later by Meliga and Reijasse.[17] First, the configuration is composed of an axisymmetric blunt body with a

a)Electronic mail: sebastien.deck@onera.fr.

 © 2009 American Institute of Physics

Downloaded 21 Jul 2009 to 144.204.16.1. Redistribution subject to AIP license or copyright; see http://pof.aip.org/pof/copyright.jsp

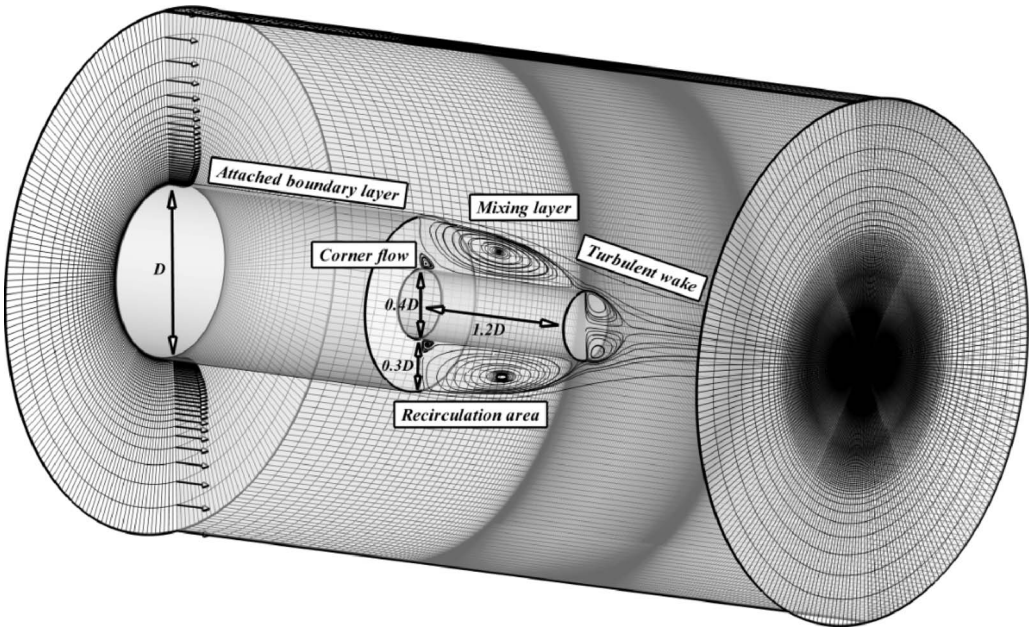

FIG. 1. Sketch of the geometry exhibiting the mesh, velocity vectors upstream from the separated area, characteristic dimensions, and the mean organization of the flow.

diameter D equal to 100 mm. This body has a 120 mm long extension which provides a L/D ratio of 1.2, where L is the emergence length, a diameter of 40 mm, and a height h for the axisymmetric step equal to 30 mm. The configuration is placed into a flow with a free stream Mach number of 0.702 yielding a Reynolds number based on the forebody diameter $\mathrm{Re}_D \approx 1.2 \times 10^6$. The initial external boundary layer thickness δ was obtained by modeling the necessary length for the forebody to have a δ/D ratio equal to 0.2.

The approach used to model the flow is zonal detached eddy simulation (ZDES) proposed by Deck[18,19] which belongs to the RANS/LES (Reynolds averaged Navier–Stokes/large eddy simulation) approaches (for more details, see the discussion of Sagaut *et al.*[20]). ZDES has been proven to be efficient in such high Reynolds number configurations to simulate complex turbulent phenomena (see Ref. 1 or Refs. 21 and 22). ZDES lets the user select RANS and DES areas. In our present case, the motivation related to the use of ZDES was to model the area downstream the separated point of the boundary layer, which is geometrically defined, with LES. Finally, the upstream part is computed using a URANS (unsteady Reynolds averaged Navier–Stokes) model, which ensures a boundary layer with the expected integral properties. As can be seen in Fig. 4(a), instable structures start to grow at the corner of the larger cylinder ($y/D=0.5$), where RANS solutions enter the LES domain. In other words, the coupling of URANS and LES ignores possible interaction of coherent structures from the oncoming boundary layer over the cylinder and the separation bubble. However, this possible interaction is assumed to be negligible which is broadly accepted for high Reynolds number massively separated flows. Indeed, on the experimental side, the issue of the reaction of turbulent flows to a sudden change in wall boundary conditions was investigated by Morris and Foss.[23] They emphasized that Holmes *et al.*[24] suggested that a communication exists between the shear layer and the separating boundary layer for laminar separation. In contrast, they argued that this is not true for high Reynolds number turbulent boundary layer. This conclusion is supported by several of their experiments. Among them, cross-correlation magnitudes between velocities measured in the boundary layer and in the entrainment stream is a strong indication that a coupling does not exist between the two regions. One can notice that in these experiments, the separation is directly due to the abrupt change in geometry and that the Reynolds number is high which is also the case in our study.

The finite-volume solver FLU3M for the compressible Navier–Stokes equations developed by ONERA has been used to perform the simulations on multiblock structured grids. The approximation of time derivatives was carried out using the Gear scheme presented by Péchier *et al.*[25] which is backward in time and second-order accurate. The spatial scheme is a modified AUSM+(P) scheme proposed by Mary and Sagaut.[26] The accuracy of the solver for DNS, LES, and hybrid RANS/LES purposes has been assessed in various applications including transitional flows around a two-dimensional wing profile in near-stall conditions (Ref. 26), afterbody flows (Ref. 27), cavity flows at high Reynolds number (Ref. 28), and synthetic jets in a cross flow (Ref. 29). In these last references, the numerical results are thoroughly compared to the available experimental data including spectral and second-order analysis.

The mesh includes almost 12×10^6 hexaedric cells, with 240 cells in the azimuthal direction (i.e., 1.5° per plan). The mesh represented in Fig. 1 is the part of interest of the whole mesh which is wider in all directions. Downstream the rear body, an O–H topology has been set to avoid singularity problem near the axis. Furthermore, as advised by Simon *et al.*,[21] the early stages of the vorticity thickness development are modeled with a 15-point-resolution which then rapidly

Downloaded 21 Jul 2009 to 144.204.16.1. Redistribution subject to AIP license or copyright; see http://pof.aip.org/pof/copyright.jsp

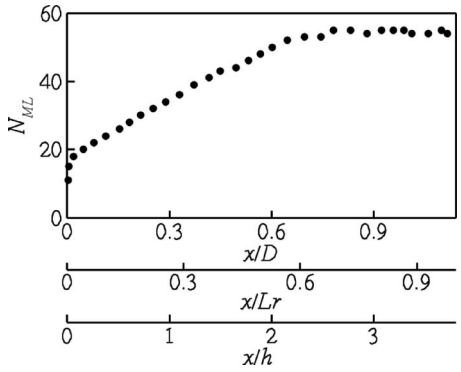

FIG. 2. Number of points N_{ML} in the vorticity thickness.

increases with the mixing layer growth up to almost a 60-point-resolution in the region of impingement of the mixing layer (see Fig. 2).

A stability analysis is carried out in the recirculation area (see Fig. 1), i.e., for $x/D \in [0;1.2]$. In this area, the flow is fully turbulent. However, in the numerical simulation, the upstream boundary layer is computed by the URANS approach. As a consequence, no turbulent structure results from the upstream flow and the coherent structures observed in the recirculation zone are directly due to the unstable character of the separated zone and/or of the mixing layer. Besides, the high Reynolds number flow and the inflectional profile nature justify the inviscid approximation for the stability analysis (see Refs. 30 and 31 for the justification of the inviscid approximation). An analysis without the inviscid approximation (not shown here for the sake of brevity) has been performed that yields identical results to the inviscid case. In the present configuration, the flow is fully turbulent. The steady axisymmetric base flow, i.e., the flow that would be observed if all perturbations were damped, is not accessible. In addition, continuation methods associated with the Newton algorithm, widely used at low Reynolds numbers to compute the base flow beyond the threshold of instability, cannot be pursued to such large Reynolds numbers. Only the mean flow can be used to assess the stability properties, keeping in mind that this mean flow is not a solution of the steady axisymmetric Navier–Stokes equations. If the nonlinear feedback is important, the stability properties differ between base and average flows. Some authors such as Hammond and Redekopp,[32] Pier,[33] Barkley,[34] and Barkley and Tuckerman[35] already studied the stability of average flow for laminar flow at low Reynolds number. Although the Reynolds number is much higher than critical Reynolds number, the stability analysis of the average flow allows to determine accurately the global frequency of the system. However, at this Reynolds regime, the stability analysis of base flow does not always allow to obtain the right flow dynamics, see Refs. 33 and 36 for a detailed discussion.

In the present paper, the mean flow [Fig. 4(b)] is computed by a double average both in time t and in azimuth θ of the ZDES solution. The general equations of motion for the instantaneous flow are the inviscid flow equations, the energy equation, written for the total energy, and the equation of state for a perfect gas. The mean flow is supposed to be weakly nonparallel, i.e., it only depends on the r direction. The present stability theory is based on the classical small perturbations technique where the instantaneous flow is the superimposition of the known mean flow and unknown fluctuations. All the physical quantities $\mathbf{q}$ (velocity, pressure, etc.) are decomposed into a mean value and an infinitesimal ($\varepsilon \ll 1$) fluctuating one. The streamwise and radial directions are both inhomogeneous directions for the mean flow [i.e., mean variables can be read $\bar{Q}(x,r)$]. In the following the classical weakly nonparallel approximation is used, and the stability of the parallel flow is considered (the dependency of the mean flow to the streamwise direction is neglected at the first order). For a cylindrical geometry the perturbation can thus be written as

$$\mathbf{q}(x,r,\theta) \equiv \bar{\mathbf{Q}}(r) + \varepsilon[\hat{\mathbf{q}}(r)\exp[i(\alpha x + m\theta - \omega t)] + \text{c.c.}]. \quad (1)$$

Finally, the linearized Euler equations lead to the well-known compressible Rayleigh equation written for the fluctuating pressure, in cylindrical geometry,

$$\frac{d^2\hat{p}}{dr^2} + \left[\frac{1}{r} - \frac{1}{\bar{\rho}}\frac{d\bar{\rho}}{dr} + \frac{2\alpha}{(\omega - \alpha\bar{U}_x)}\frac{d\bar{U}_x}{dr}\right]\frac{d\hat{p}}{dr} + \left[\bar{\rho}(\alpha\bar{U}_x - \omega)^2 M^2 - \left(\alpha^2 + \frac{m^2}{r^2}\right)\right]\hat{p} = 0\,. \quad (2)$$

The boundary condition imposed in the present problem expresses that fluctuations do not vary far from the afterbody and the viscosity is not considered at the wall.

The compressible Rayleigh equation is integrated using a spectral collocation based on the Chebychev Gauss-Lobatto points. Details of the numerical method used to discretize Eq. (2) are specified in Ref. 37. The resulting complex nonsymmetric generalized eigenvalue problem is solved by using the direct LAPACK eigenvalue solver, which computes the whole spectrum of eigenvalues of the discretized operator. Newton–Raphson algorithm is eventually used to follow spatial branches of solutions.

III. RESULTS AND DISCUSSION

A. Validation

The unsteady aerodynamic field is time-averaged during the calculation. The mean streamwise pressure coefficient at the wall $Cp = (P - P_\infty)/\frac{1}{2}\rho_\infty U_\infty^2$ is depicted in Fig. 3(a) as a function of the location along the emerging body nondimensioned by three characteristic length scales, i.e., D the diameter of the larger cylinder, h the step height, and L_r the reattachment length. This figure allows to differentiate three regions described in Ref. 1 on the same axisymmetric configuration with a supersonic jet. For $x/L_r \leq 0$, a slow decrease in Cp as the streamwise location increases highlights the upstream influence of the recirculation region on the main body. The second region shows a small decrease in Cp in the separation region from $x=0$ up to $x=L_r/2$ due to the acceleration of the backflow. The last region is characterized by a strong recompression process where the amplitude $Cp_{\max}$ is reached downstream the mean reattachment point at $x/L_r \approx 1.15$. The location of the reattachment is $x_r \approx 1.15D$

Downloaded 21 Jul 2009 to 144.204.16.1. Redistribution subject to AIP license or copyright; see http://pof.aip.org/pof/copyright.jsp

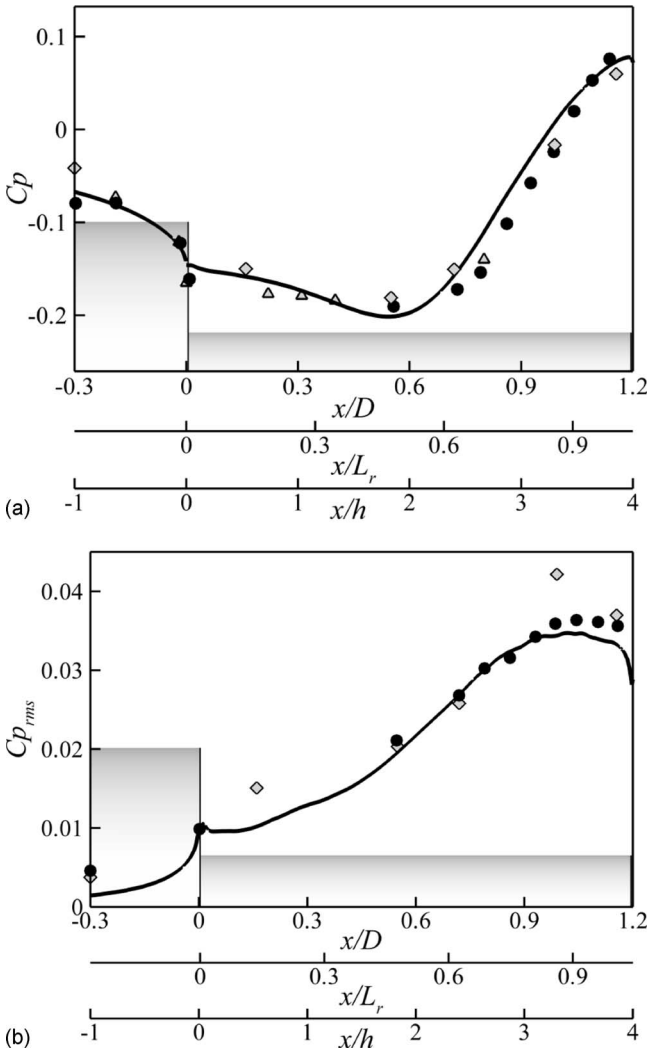

FIG. 3. (a) Streamwise distribution of the pressure coefficient. (◇) Ref. 6 (kulites), (△) Ref. 6 (steady taps), (●) Ref. 17, and (–) present case. (b) Streamwise distribution of the coefficient of rms pressure fluctuation. (◇) Ref. 6 (kulites), (●) Ref. 17, and (–) present case.

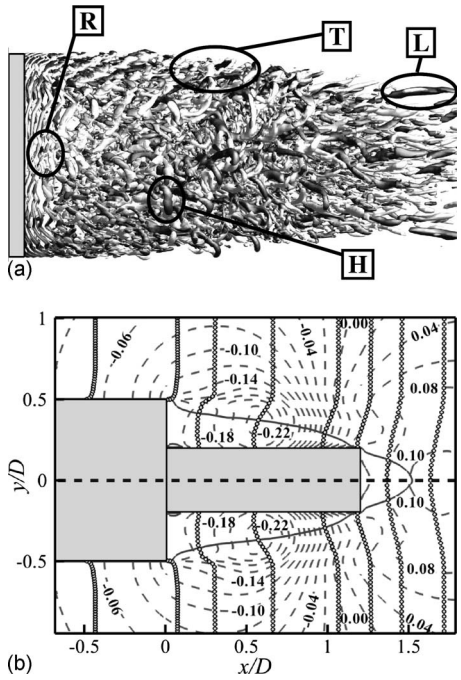

FIG. 4. (a) Snapshot of the coherent structures downstream of the step flow with their rotation visualized with an isosurface of $QU_\infty^2/D^2=50$ colored by the sign of streamwise vorticity (white for positive and gray for negative). (b) time-averaged flow field. (– –) Iso-Cp with $\Delta C_p=0.02$ between two lines, (–) isovelocity $U/U_\infty=0.01$, and (○) velocity profiles at several streamwise locations.

and the dimensions of the recirculation zone is materialized with a continuous line [see Fig. 4(b)] as well as some velocity profiles along the configuration and iso-Cp contours in the flow field corroborating the values at the wall. Finally, it is worth mentioning that Cp values are in excellent agreement with the experimental data of Deprés *et al.*[6] and Meliga and Reijasse[17] on analogous configurations.

The root-mean-square coefficient of the pressure fluctuation $Cp_{\mathrm{rms}}=\overline{P'^2}/\frac{1}{2}\rho_\infty U_\infty^2$, where $\overline{P'^2}$ is the fluctuating pressure is shown at the wall in Fig. 3(b). The fluctuation level increases steadily in the streamwise direction downstream the base and reaches a plateau just upstream from the mean shear layer reattachment location ($Cp_{\mathrm{rms}}\approx 0.035$) which was confirmed by the recent experiment of Meliga and Reijasse[17] at $x/L_r\approx 0.9$. Let us be reminded that Hudy *et al.*[38] linked this growth in rms to the organized shear layer structures which get stronger and move closer to the wall.

The behavior of the instantaneous flow field is illustrated in Fig. 4(a). The turbulent structures are evidenced plotting a positive isovalue of the second invariant of the velocity gradient tensor defining vortex tubes. In addition, the rotation is shown through the coloring of these tubes with the sign of the streamwise vorticity (white for positive and gray for negative).

A roll-up (R) of toroidal eddies apparently occurs apparying and rapidly replaced by large three-dimensional structures (T). They develop as the shear layer approaches reattachment and are destabilized by azimuthal instability modes according to Deck and Thorigny.[1] Furthermore, the occurrence of large scale hairpin vortices (H) in the reattachment zone is shown. After the break up of the eddies the main structures appear to be longitudinal eddies (L). Some similarities with the axisymmetric bluff body discussed by Sandberg and Fasel[16] such as oblique or helical structures, longitudinal structures, and several vortex loops can be noticed. However, their scales differ because the convective Mach number and the Reynolds number are quite different. Furthermore, low frequency dynamics of the flow seems to be controlled by the first and not by the second detachment of the near wake like in Ref. 16.

B. Spectral analysis

Regarding the various scales and phenomena qualitatively observable in the instantaneous flow field, it appears that the complexity of the flow could be partially uncovered through the scrutiny of the unsteady properties of the flow. Following this compass, Fig. 5 displays a linear-log axis plot of the contribution to the total energy of a peculiar frequency band thanks to the estimated power spectral density (PSD) function of pressure fluctuations, named $G(f)$. This pressure

Downloaded 21 Jul 2009 to 144.204.16.1. Redistribution subject to AIP license or copyright; see http://pof.aip.org/pof/copyright.jsp

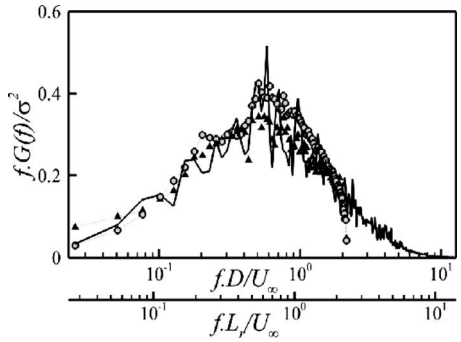

FIG. 5. Normalized premultiplied PSD of the pressure at the wall for the streamwise location $x/D=0.99$. (○) Ref. 17, (▲) Ref. 6, and (–) present calculation.

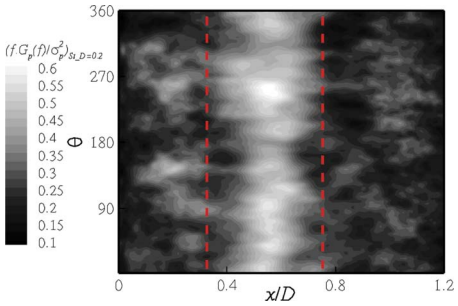

FIG. 6. (Color online) Spectral sheet of normalized premultiplied PSD of the pressure fluctuations at the wall $fG_p(f)/\sigma_p^2$ for every streamwise and azimuthal locations along the emergence and for the particular dimensionless frequency $\mathrm{St}_D=0.2$. (– –) Spatial limits of the absolute area for $m=1$.

spectrum, located at the station $x/D=0.99$ among the rear body is represented with a solid line and compared to the available experiments of Deprés *et al.*[6] and Meliga and Reijasse[17] symbolized with a triangle and an open circle, respectively. One can notice that the broadband spectrum is well reproduced by the simulation.

This broadband high frequency contribution prevails upon the spectrum since the organized shear layer structures, which grow in strength, move closer to the wall before crashing against it and breaking into smaller scales. Note also that this broadband contribution is centered around $fL_r/U_\infty \approx 0.6$, which agrees with the earlier conclusions of Mabey.[39] This is the characteristic frequency of vortical structures seen in free shear layers. In addition, this spectrum displays a peak at $fL_r/U_\infty \approx 0.1$ close to former observations in two-dimensional separating/reattaching flows (see Ref. 40 for instance). This low frequency peak is often attributed (see Ref. 41) to the "flapping" of the shear layer and reflects the overall separation-bubble growth/decay dynamics. Finally, the presence of the well-known "shedding" appears through a peak near $fD/U_\infty \approx 0.2$.

In order to evidence the relationship between the frequencies of the absolutely unstable waves and those given by the eigenvalue problem, PSDs of the pressure fluctuations at the wall have been plotted for the whole flow field on the emergence. In addition, values of the energy at the particular dimensionless frequency $\mathrm{St}_D=0.2$ have been selected and reported on the map $G(x/D,\theta)$ shown in Fig. 6. It appears that the spatial location of the Strouhal number $\mathrm{St}_D=0.2$ matches well the absolute instability location provided by the eigenvalue problem which constitutes a first step toward the identification of the antisymmetric mode ($m=1$).

To get deeper insight into the spatial organization of the flow at these frequencies, the azimuthal coherence of two pressure sensors $p_1(r,x,\phi_1)$ and $p_2(r,x,\phi_2)$ located in a plane normal to the inflow at a constant position x and a constant radius r can be considered. Assuming the hypothesis of an homogeneous flow, i.e., without any preferred angle of reference ϕ_1, the complex coherence function may be expressed as

$$C(f,r,x,\Delta\phi) = (C_r + jC_i)(f,r,x,\Delta\phi) = \frac{S_{12}(f,r,\Delta\phi,x)}{\sqrt{S_1(f,r,\phi_1,x)S_2(f,r,\phi_2,x)}}, \tag{3}$$

where $j=\sqrt{-1}$, and C_r and C_i are the real and imaginary part of the cross-spectral density function S_{12} and $\Delta\phi=\phi_1-\phi_2$, respectively. Assuming that the disturbances do not exhibit any particular direction of propagation, one has $S_{12}(\Delta\phi)=S_{12}(-\Delta\phi)$. Besides, the hypothesis of isotropy yields $C_i=0$. Consequently, the C_r function is 2π periodic with respect to $\Delta\phi$ and can be expressed as, thanks to a Fourier transform in azimuthal modes,

$$C_r(f,\Delta\phi) = \sum_{m=0}^{\infty} C_{r,m}(f)\cos(m\Delta\phi). \tag{4}$$

$C_{r,m}$ represents the percentage of the fluctuating energy at frequency f relative to the azimuthal mode m since $\Sigma_m C_{r,m}=1$. Let us be reminded that $m=0$ and $m=1$ modes are characterized by an in phase and antiphase relationship of signals, respectively, recorded simultaneously at two diametrically opposed locations. Figures 7(a)–7(h) show the $C_{r,m}$ spectrum for the first four azimuthal modes ($m\in[|0-3|]$) at the streamwise locations $x/D=1.15$ and $x/D=0.72$ in the separated area. One can notice the very good agreement with the experimental data by Deprés *et al.*[6](black triangles) and Meliga and Reijasse[17] (black bullets). The $m=0$ contribution is confined at low frequencies and decreases continuously with increasing frequencies which is due to the low flapping frequency of the shear layer (see Ref. 1). The spectrum $C_{r,1}$ at $0.72D$ displays a peak near $fD/U_\infty \approx 0.2$ and shows that experimentally more than 80% of the pressure fluctuations at this specific frequency are due to this antisymmetric mode. Figures 7(e) and 7(f) clearly illustrate the fact that the energy related to the dimensionless frequency $fD/U_\infty \approx 0.2$ has mainly been redistributed from the axisymmetric $m=0$ mode to the antisymmetric $m=1$ mode. Then, as represented in Figs. 7(c), 7(d), 7(g), and 7(h), for higher modes ($m>1$) no particular frequency contributes for a significant amount of energy in the fluctuations. Then, a $C_{r,m}$ spectrum has been plotted for every streamwise location

Downloaded 21 Jul 2009 to 144.204.16.1. Redistribution subject to AIP license or copyright; see http://pof.aip.org/pof/copyright.jsp

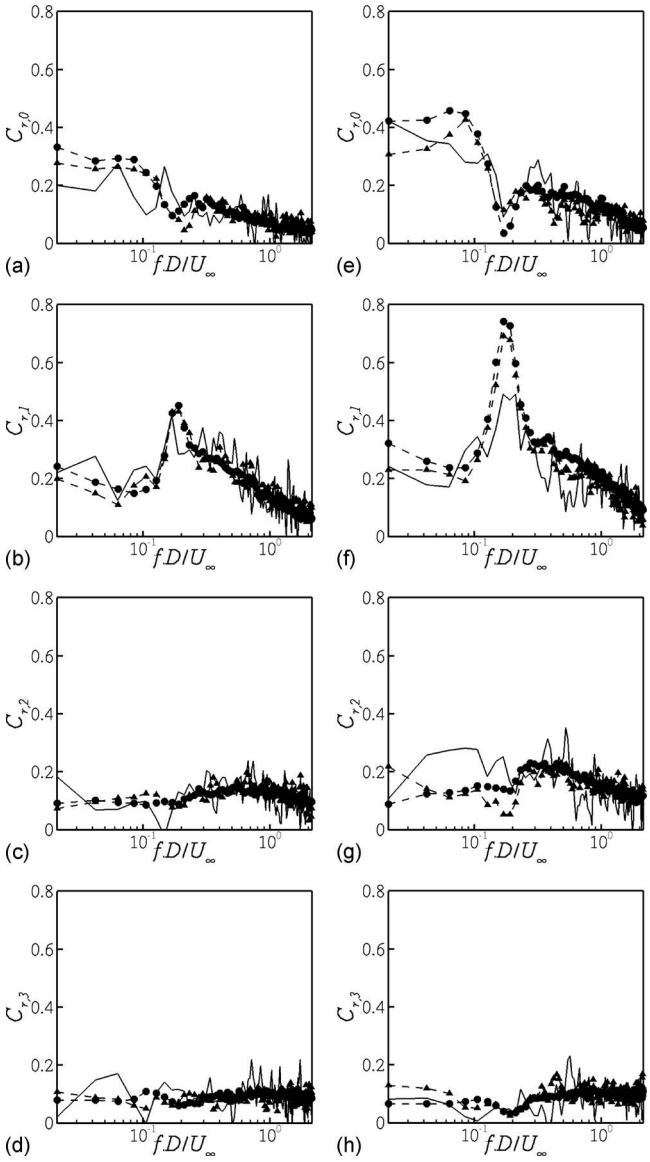

FIG. 7. [(a)–(d)] Spectra of the first four azimuthal pressure modes $C_{r,0}$, $C_{r,1}$, $C_{r,2}$, and $C_{r,3}$ for the streamwise location $x/D=1.15$. (▲) Ref. 6, (●) Ref. 17, and (–) present calculation. [(e)–(h)] Spectra of the first four azimuthal pressure modes $C_{r,0}$, $C_{r,1}$, $C_{r,2}$, and $C_{r,3}$ for the streamwise location $x/D=0.72$. (▲) Ref. 6, (●) Ref. 17, and (–) present calculation.

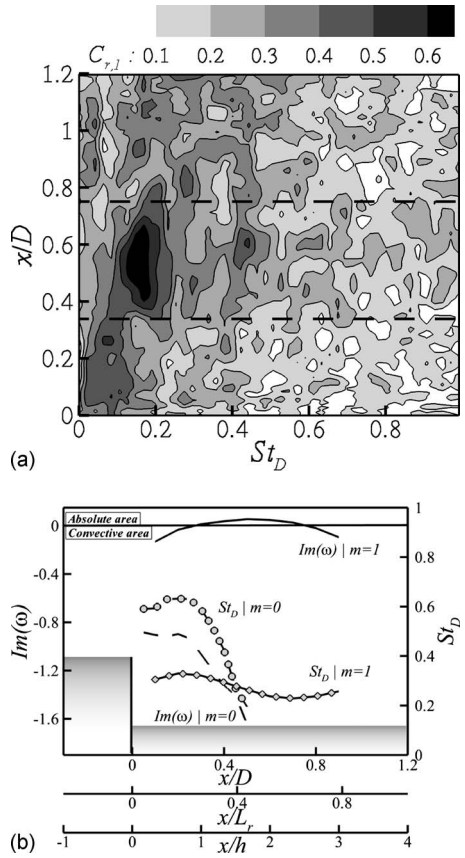

FIG. 8. (a) Spectral sheet of the azimuthal pressure mode $C_{r,1}$ for every streamwise location along the emergence in function of nondimensional frequencies; (– –) spatial limits of the absolute area for $m=1$. (b) $m=0$ and $m=1$ modes for the axisymmetric case; (– –) $\mathrm{Im}(\omega)^{m=0}=f(x/D,x/L_r,x/h)$, (–) $\mathrm{Im}(\omega)^{m=1}=f(x/D,x/L_r,x/h)$, (○) $\mathrm{St}_D^{m=0}=f(x/D,x/L_r,x/h)$, and (◇) $\mathrm{St}_D^{m=1}=f(x/D,x/L_r,x/h)$.

providing a spectral layer [Fig. 8(a)]. It exhibits the highest percentages of the fluctuating energy for Strouhal numbers St_D based on the forebody diameter close to 0.2 and which are localized between $x/D\approx 0.35$ and $x/D\approx 0.75$. Let us now consider a perturbation approach of this flow.

In the context of spatiotemporal stability analysis, the singularities of the resulting dispersion relation are determined and the ones satisfying the Briggs–Bers (Refs. 42 and 43) pinching criterion have been selected. Frequency-wavenumber pair (ω_0,α_0) solutions to the dispersion relation [i.e., $\omega_0(\alpha_0)=0$] and corresponding to the zero group velocity [i.e., $\partial\omega/\partial\alpha(\alpha_0)=0$] are prospected by an iterative Newton–Raphson algorithm. Results are summarized in Fig. 8(b). Figure 8(b) shows the streamwise evolution of the Strouhal number St_D based on the diameter of the larger cylinder (circles stand for mode $m=0$ and diamonds are for mode $m=1$) and of the absolute growth rate $\mathrm{Im}(\omega)$ (dashed line is for $m=0$ and solid line is for $m=1$) along the extension. The solid horizontal line denotes the threshold of marginal absolute instability $\mathrm{Im}(\omega)=0$. The mean flow appears to be linearly absolutely stable for an axisymmetric disturbance ($m=0$) for all streamwise locations and frequencies. Concerning a helical disturbance ($m=1$), well represented in Ref. 44, mean flow is linearly absolutely unstable for a broad range of abscissa $x/D\in[0.35;0.75]$ close to $\mathrm{St}_D\approx 0.2$. The coexistence of absolute helicoidal ($m=1$) unstable global modes within the recirculation region and convectively unstable shear layer modes corroborates the results of Sandberg and Fasel.[16] To be able to compare with the previous ZDES results, it is necessary to determine if the flow is linearly globally unstable because being absolutely unstable is only necessary but not a sufficient condition (Ref. 45). Different selection criteria for the global frequency, ω_g, whose success depends on the type of considered flow, have been proposed in the past, i.e., Pierrehumbert[46] for the maximum growth criterion, Koch[47] for the hydrodynamic resonance criterion, and Monkewitz and Nguyen[48] for the initial growth criterion. In the 1990s, the study of linear global stability of weakly nonparallel shear flows provided the first criterion based on solid theoretical grounds, Ref. 45. More recently, in the framework of the fully nonlinear Navier–Stokes equations,

Downloaded 21 Jul 2009 to 144.204.16.1. Redistribution subject to AIP license or copyright; see http://pof.aip.org/pof/copyright.jsp

the frequency selection criterion was obtained by Pier and Huerre[49] which generalized the initial growth criterion.

In this present compressible turbulent afterbody flow the linear frequency selection criterion (Ref. 45) is given by

$$\omega_g = \omega_0(X_s) \quad \text{and} \quad \frac{\partial \omega_0}{\partial X_s} = 0, \tag{5}$$

where X_s represents a saddle point in the complex X-plane. However, since derivatives of $\omega(X)$ are only known along the real x-axis, the location of the saddle point X_s of $\omega(X)$ was found through use of the Cauchy–Riemann equations and analytic continuation to complex values of $X=x_r+ix_i$. Details of the method used are described in Ref. 32. Finally, the location of the saddle point for this flow is $X_s/D=0.502+6.7\times10^{-3}i$ nearly on the real x-axis and close to the location of the maximum absolute growth rate. The linear selection criterion provides the best accuracy regarding the Strouhal number observed in numerical simulations. Indeed, this linear criterion points out that the dominant global mode is close to $\mathrm{St}_D=0.227$ which is in perfect agreement with ZDES results ($\mathrm{St}_D\simeq0.2$ on Fig. 5) while the nonlinear criterion gives $\mathrm{St}_D=0.325$. The fact that stability analysis uses the average flow and not the base flow is a possible explanation of this result. Pier[33] showed for the cylinder wake at low Reynolds numbers, when the average flow is used, that the criterion of Chomaz *et al.*[45] gave an excellent result. Apparently, although the Reynolds number is high, the presence of the wall significantly reduces the absolute instability leading to the global mode frequency selection by the linear criterion and not by the nonlinear criterion. On the other hand, the spectrum of the azimuthal antisymmetric pressure mode, depicted in Fig. 8(a), finds a maximum of fluctuating energy precisely in the absolutely unstable area of the mean flow.

Figure 9(a) illustrates the streamwise variations of the absolute wavelength (symbolized by inverted triangles) defined as $\lambda_0=2\pi/\mathrm{Re}(k)$, where $\mathrm{Re}(k)$ is the real part of the absolute wavenumber, and of the absolute growth rate $\mathrm{Im}(w)$ (solid line). The absolute wavelength at the location of the absolute frequency predicted with the linear frequency criterion is equal to $2.05D$.

One can now consider an instantaneous pressure field $p(r,\theta,z)$ which is decomposed into azimuthal Fourier series according to the following expression: $p(r,\theta,z)=\Sigma_m p_m(r,z)e^{im\theta}$. Figure 9(b) represents the real part of the pressure coefficient $\mathrm{Re}(p)$ for the $m=1$ component. Near the separation region, small scale structures are visible becoming alternated large scale structures downstream the emergence.

The absolute wavelength shown in Fig. 9(a) compares well with the spatial distribution observed in Fig. 9(b). Such an agreement between the decomposition into azimuthal Fourier series and the absolute wavelength resulting from the local stability analysis was observed by Meliga[50] for a blunt-based bluff body featuring a fluidic reattachment. These clear agreements show that the dynamics of the axisymmetric afterbody is dominated by a global instability phenomenon at least for this regime.

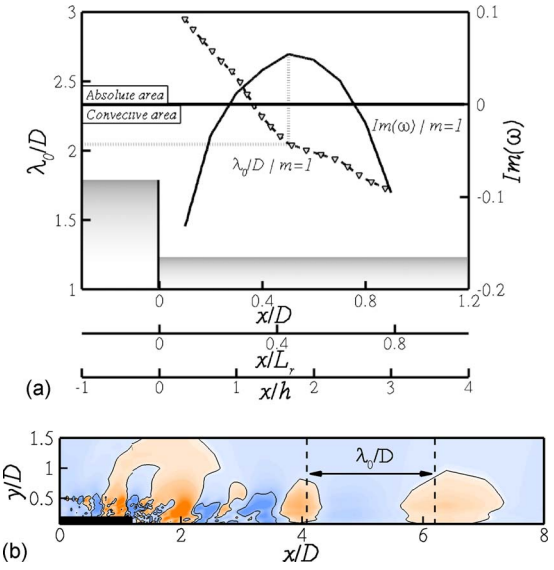

FIG. 9. (Color online) (a) Streamwise evolution (▽) of the absolute wavelength $\lambda_0=f(x/D,x/L_r,x/h)$ and (–) of the absolute growth rate $\mathrm{Im}(\omega)^{m=1}=f(x/D,x/L_r,x/h)$. The dotted lines stand for the wavelength which corresponds to the absolute growth rate given by the linear frequency selection criterion. (b) Instantaneous spatial structure visualized for the $m=1$ component of the real part of the pressure coefficient $\mathrm{Re}(p)$ with the absolute dimensionless wavelength λ_0/D.

IV. CONCLUSIONS

Axisymmetric turbulent separating/reattaching flow has been investigated at $\mathrm{Re}_D\approx1.2\times10^6$. First the simulation is well validated considering the very good agreement between the Reynolds averaged data as well as the spectral content and the experiments.

It is shown that a large scale coherent motion at frequency $fD/U_\infty\approx0.2$ dominates an ordered structure in this separating/reattaching flow. These results corroborate the experiments of Deprés *et al.*[6] and Meliga and Reijasse.[17] The stability analysis has allowed us to show that axisymmetric turbulent afterbody dynamics is clearly dominated by a helical absolute instability while other modes ($m=0$ and $m\geq2$) remain of convective nature. These results are in excellent agreement with the azimuthal antisymmetric pressure mode spectra. This last point is of major importance since the analysis of the flow dynamics and the perturbation technique converge on the same spatial information.

In future work, it would be interesting to relax the weakly nonparallel hypothesis of the actual stability analysis by studying directly the global stability of such flow. An example of such a possible approach is described in Ref. 51. The knowledge of the main mechanisms governing the flow dynamics opens interesting perspectives of flow control. Indeed, considering the localized absolute area as a receptive zone, the use of any passive or active device in this area could be the most efficient in modifying the flow physics. The suppression of the absolute zone might modify the instability nature of the flow from absolute to convective and hence eliminate the low frequency dynamics.

Downloaded 21 Jul 2009 to 144.204.16.1. Redistribution subject to AIP license or copyright; see http://pof.aip.org/pof/copyright.jsp

ACKNOWLEDGMENTS

The authors thank the Centre National d'Etudes Spatiales (CNES) for financial support within the framework of the research and technology program ATAC (aerodynamics of nozzles and afterbodies). The Ph.D. work of P. E. Weiss was funded by CNES and ONERA.

[1] S. Deck and P. Thorigny, "Unsteadiness of an axisymmetric separating-reattaching flow," Phys. Fluids **19**, 065103 (2007).
[2] A. Roshko, "On the wake and drag of bluff bodies," J. Aeronaut. Sci. **22**, 124 (1955).
[3] J. R. Calvert, "Experiments on low speed flow past cones," J. Fluid Mech. **27**, 273 (1967).
[4] S. L. Gai and S. R. Patil, "Subsonic axisymmetric base flow experiments with base modifications," J. Spacecr. Rockets **17**, 42 (1980).
[5] J. Délery and M. Siriex, "Base flows behind missiles," ONERA Technical Report No. AGARD LS-98, 1979.
[6] D. Deprés, P. Reijasse, and J. P. Dussauge, "Analysis of unsteadiness in afterbody transonic flows," AIAA J. **42**, 2541 (2004).
[7] A. Roshko, "Structure of turbulent shear flows: A new look," AIAA J. **14**, 1349 (1976).
[8] J. Laufer, "New trend in experimental turbulence research," Annu. Rev. Fluid Mech. **7**, 307 (1975).
[9] B. J. Cantwell, "Organized motion in turbulent flow," Annu. Rev. Fluid Mech. **13**, 457 (1981).
[10] C. M. Ho and P. Huerre, "Perturbated free shear layer," Annu. Rev. Fluid Mech. **16**, 365 (1984).
[11] A. K. M. F. Hussain and W. C. Reynolds, "The mechanics of an organized wave in turbulent shear flow," J. Fluid Mech. **41**, 241 (1970).
[12] A. K. M. F. Hussain and W. C. Reynolds, "The mechanics of an organized wave in turbulent shear flow. Part 2. Experimental results," J. Fluid Mech. **54**, 241 (1972).
[13] W. C. Reynolds and A. K. M. F. Hussain, "The mechanics of an organized wave in turbulent shear flow. Part 3. Theoretical models and comparisons with experiments," J. Fluid Mech. **54**, 263 (1972).
[14] D. Wee, T. Yi, A. Annaswamy, and A. F. Ghoniem, "Self-sustained oscillations and vortex shedding in backward-facing step flows: Simulation and linear instability analysis," Phys. Fluids **16**, 3361 (2004).
[15] Y. Lifshitz, D. Degani, and A. Tumin, "Coherent perturbations in a turbulent boundary layer subjected to a highly adverse pressure gradient," AIAA Paper No. 2005-4809, June 2005.
[16] R. D. Sandberg and H. F. Fasel, "Numerical investigation of transitional supersonic axisymmetric wakes," J. Fluid Mech. **563**, 1 (2006).
[17] P. Meliga and P. Reijasse, "Unsteady transonic flow behind an axisymmetric afterbody with two boosters," Proceedings of the 25th AIAA Applied Aerodynamics Conference, Miami, June 2007, Paper No. 2007-4564.
[18] S. Deck, "Zonal-detached-eddy simulation of the flow around a high-lift configuration," AIAA J. **43**, 2372 (2005).
[19] S. Deck, "Numerical simulation of transonic buffet over a supercritical airfoil," AIAA J. **43**, 1556 (2005).
[20] P. Sagaut, S. Deck, and M. Terracol, *Multiscale and Multiresolution Approaches in Turbulence* (Imperial College Press, London, 2006).
[21] F. Simon, S. Deck, P. Guillen, P. Sagaut, and A. Merlen, "Numerical simulation of the compressible mixing layer past an axisymmetric trailing edge," J. Fluid Mech. **591**, 215 (2007).
[22] F. Simon, S. Deck, Ph. Guillen, and P. Sagaut, "Reynolds averaged Navier Stokes/large eddy simulations of supersonic base flow," AIAA J. **44**, 2578 (2006).
[23] S. C. Morris and J. F. Foss, "Turbulent boundary layer to single-stream shear layer: The transition region," J. Fluid Mech. **494**, 187 (2003).
[24] P. Holmes, J. L. Lumley, and G. Berkooz, *Coherent Structures, Symmetry: Dynamical Systems and Turbulence* (Cambridge University Press, Cambridge, 1992).
[25] M. Péchier, P. Guillen, and R. Caysac, "Magnus effect over finned projectiles," J. Spacec. Rockets **38**, 542 (2001).
[26] I. Mary and P. Sagaut, "Large eddy simulation of flow around an airfoil near stall," AIAA J. **40**, 1139 (2002).
[27] S. Deck, E. Garnier, and P. Guillen, "Turbulence modelling applied to space launcher configurations," J. Turbul. **3**, 57 (2002).
[28] L. Larchevêque, P. Sagaut, I. Mary, and O. Labbé, "Large-eddy simulation of a compressible flow past a deep cavity," Phys. Fluids **15**, 193 (2003).
[29] J. Dandois, E. Garnier, and P. Sagaut, "Numerical simulation of active separation control by a synthetic jet," J. Fluid Mech. **574**, 25 (2007).
[30] W. Blumen, P. G. Drazin, and D. F. Billings, "Shear layer instability of an inviscid compressible fluid. Part 2," J. Fluid Mech. **71**, 305 (1975).
[31] P. Huerre and P. A. Monkewitz, "Absolute and convective instabilities in free shear layer," J. Fluid Mech. **159**, 151 (1985).
[32] D. Hammond and L. Redekopp, "Global dynamics of symmetric and asymmetric wakes," J. Fluid Mech. **331**, 231 (1997).
[33] B. Pier, "On the frequency selection of finite-amplitude vortex shedding in the cylinder wake," J. Fluid Mech. **458**, 407 (2002).
[34] D. Barkley, "Linear analysis of the cylinder wake mean flow," Europhys. Lett. **75**, 750 (2006).
[35] D. Barkley and L. S. Tuckerman, "Mean flow of turbulent-laminar patterns in plane Couette flow," J. Fluid Mech. **576**, 109 (2007).
[36] D. Sipp and A. Lebedev, "Global stability of base and mean flows: A general approach and its applications to cylinder and open cavity flows," J. Fluid Mech. **593**, 333 (2007).
[37] J.-Ch. Robinet, J.-P. Dussauge, and G. Casalis, "Wall effect on the convective-absolute boundary for the compressible shear layer," Theor. Comput. Fluid Dyn. **15**, 143 (2001).
[38] L. M. Hudy, A. M. Naguib, and W. M. Humphreys, "Wall-pressure-array measurements beneath a separating/reattaching flow region," Phys. Fluids **15**, 706 (2003).
[39] D. G. Mabey, "Pressure fluctuations caused by separated bubble flows at subsonic speeds," Royal Aircraft Establishment Technical Report No. RAE-TR-71160, 1971.
[40] I. Lee and H. J. Sung, "Characteristics of wall pressure fluctuations in separated and reattaching flows over a backward-facing step: Part 1. Time-mean statistics and cross-spectral analyses," Exp. Fluids **30**, 262 (2001).
[41] D. M. Driver, H. L. Seegmiller, and J. Marvin, "Time-dependent behavior of a reattaching shear layer," AIAA J. **25**, 914 (1987).
[42] R. J. Briggs, *Electron-Stream Interaction With Plasmas* (MIT, Cambridge, 1964).
[43] A. Bers, in *Physique des Plasmas*, edited by C. Dewitt and J. Peyraud (Gordon and Breach, New York, 1975), p. 117.
[44] A. Weickgenannt and P. A. Monkewitz, "Control of vortex shedding in an axisymmetric bluff body wake," Eur. J. Mech. B/Fluids **19**, 789 (2000).
[45] J.-M. Chomaz, P. Huerre, and L. M. Redekopp, "A frequency selection criterion in spatially developing flows," Stud. Appl. Math. **84**, 119 (1991).
[46] R. T. Pierrehumbert, "Local and global baroclinic instability of zonally varying flow," J. Atmos. Sci. **41**, 2141 (1984).
[47] W. Koch, "Local instability characteristics and frequency determination of self-excited wake flows," J. Sound Vib. **99**, 53 (1985).
[48] P. A. Monkewitz and L. N. Nguyen, "Absolute instability in the near-wake of two-dimensional bluff bodies," J. Fluids Struct. **1**, 165 (1987).
[49] B. Pier and P. Huerre, "Nonlinear self-sustained structures and fronts in spatially developing wake flows," J. Fluid Mech. **435**, 145 (2001).
[50] P. Meliga, "A theoretical approach for the onset and control of unsteadiness in compressible afterbody flows," Ph.D. thesis, Ecole Polytechnique, 2008.
[51] J.-Ch. Robinet, "Bifurcations in shock wave/laminar boundary layer interaction: Global instability approach," J. Fluid Mech. **579**, 85 (2007).

Downloaded 21 Jul 2009 to 144.204.16.1. Redistribution subject to AIP license or copyright; see http://pof.aip.org/pof/copyright.jsp